

DFTT 18/99  
 ROM2F/99/07  
 LAPTH-727/99  
 FTUV/99-22  
 IFIC/99-23

## Extending the DAMA annual-modulation region by inclusion of the uncertainties in astrophysical velocities

P. Belli<sup>a\*</sup>, R. Bernabei<sup>a</sup>, A. Bottino<sup>b</sup>, F. Donato<sup>c</sup>,  
 N. Fornengo<sup>d</sup>, D. Prosperi<sup>e</sup>, S. Scopel<sup>f†</sup>

<sup>a</sup> *Dipartimento di Fisica, Università di Roma “Tor Vergata”  
 and INFN, Sez. di Roma2, I-00133 Roma, Italy*

<sup>b</sup> *Dipartimento di Fisica Teorica, Università di Torino  
 and INFN, Sez. di Torino, Via P. Giuria 1, I-10125 Torino, Italy*

<sup>c</sup> *Laboratoire de Physique Théorique LAPTH, B.P. 110, F-74941  
 Annecy-le-Vieux Cedex, France*

*and INFN, Sez. di Torino, Via P. Giuria 1, I-10125 Torino, Italy*

<sup>d</sup> *Instituto de Física Corpuscular – C.S.I.C. – Departamento de Física Teòrica,  
 Universitat de València, E-46100 Burjassot, València, Spain*

<sup>e</sup> *Dipartimento di Fisica, Università di Roma “La Sapienza”  
 and INFN, Sez. di Roma, I-00185, Roma, Italy*

<sup>f</sup> *Instituto de Física Nuclear y Altas Energías, Facultad de Ciencias,  
 Universidad de Zaragoza, Plaza de San Francisco s/n, E-50009 Zaragoza, Spain*

### Abstract

The original annual-modulation region, singled out by the DAMA/NaI experiment for direct detection of WIMPs, is extended by taking into account the uncertainties in the galactic astrophysical velocities. Also the effect due to a possible bulk rotation for the dark matter halo is considered. We find that the range for the WIMP mass becomes  $30 \text{ GeV} \lesssim m_\chi \lesssim 130 \text{ GeV}$  at  $1-\sigma$  C.L. with a further extension in the upper bound, when a possible bulk rotation of

---

\*E-mail: belli@roma2.infn.it, bernabei@roma2.infn.it, bottino@to.infn.it, donato@lapp.in2p3.fr, prosperi@roma1.infn.it, fornengo@flamenco.ific.uv.es, scopel@posta.unizar.es

†INFN Post-doctoral Fellow

the dark matter halo is taken into account. We show that the DAMA results, when interpreted in the framework of the Minimal Supersymmetric extension of the Standard Model, are consistent with a relic neutralino as a dominant component of cold dark matter (on the average in our universe and in our galactic halo). It is also discussed the discovery potential for the relevant supersymmetric configurations at accelerators of present generation.

## I. INTRODUCTION

The DAMA/NaI Collaboration has recently reported the indication of an annual-modulation effect in a direct search experiment for WIMPs [1–3]. In Ref. [3] it has been shown that a statistical (maximum-likelihood) analysis of the data concerning to a total exposure of  $19,511 \text{ kg} \times \text{day}$  provides, at a  $2\text{-}\sigma$  C.L., a well delimited region in the plane  $\rho_\chi \sigma_{\text{scalar}}^{(\text{nucleon})} - m_\chi$ , where  $m_\chi$  is the WIMP mass,  $\rho_\chi$  is its local (solar neighbourhood) density and  $\sigma_{\text{scalar}}^{(\text{nucleon})}$  is the WIMP-nucleon scalar elastic cross section. Obviously, the location of the annual-modulation region depends on the functional form adopted for the speed distribution of the dark matter particles, and on the values assigned to the galactic astrophysical velocities. In Refs. [1–3] a standard Maxwellian distribution was taken for the WIMP speed distribution with a root mean square velocity  $v_{\text{rms}} = 270 \text{ Km s}^{-1}$  and a WIMP escape velocity in the halo  $v_{\text{esc}} = 650 \text{ Km s}^{-1}$ .

The DAMA/NaI results on annual-modulation were analyzed in Refs. [4–8] in terms of relic neutralinos. It was proved that the DAMA/NaI data are compatible with a neutralino as a major component of dark matter in the universe. In Refs. [4–8] it was also shown that a significant number of the relevant supersymmetric configurations are compatible with supergravity schemes [9], are explorable at accelerators and/or by indirect searches for relic particles (up-going muons at neutrino telescopes and antiprotons in space).

In the present paper we discuss: i) the extension of the DAMA/NaI annual-modulation region in the plane  $\rho_\chi \sigma_{\text{scalar}}^{(\text{nucleon})} - m_\chi$ , when the uncertainties of the galactic astrophysical velocities are taken into account, and ii) the ensuing consequences of this extension in terms of properties for relic neutralinos and for the related supersymmetric configurations [10].

## II. EXTENDED ANNUAL-MODULATION REGION

The differential rate for WIMP direct detection is given by

$$\frac{dR}{dE_R} = N_T \frac{\rho_\chi}{m_\chi} \int_{v_{\text{min}}}^{v_{\text{max}}} d\vec{v} f(\vec{v}) v \frac{d\sigma}{dE_R}(v, E_R), \quad (1)$$

where  $N_T$  is the number of the target nuclei per unit of mass,  $\vec{v}$  and  $f(\vec{v})$  denote the WIMP velocity and velocity distribution function in the Earth frame ( $v = |\vec{v}|$ ) and  $d\sigma/dE_R$  is the WIMP-nucleus differential cross section. The nuclear recoil energy is given by  $E_R = m_{\text{red}}^2 v^2 (1 - \cos \theta^*) / m_N$ , where  $\theta^*$  is the scattering angle in the WIMP-nucleus center-of-mass frame,  $m_N$  is the nuclear mass and  $m_{\text{red}}$  is the WIMP-nucleus reduced mass. The velocity  $v_{\text{min}}$  is defined as  $v_{\text{min}} = (m_N E_R / 2m_{\text{red}}^2)^{\frac{1}{2}}$  and  $v_{\text{max}}$  is the maximal (escape) WIMP velocity in the Earth reference frame. Eq.(1) refers to a mono-atomic detector; the generalization to our case of NaI is straightforward.

In principle, the differential WIMP-nucleus cross section is composed of a coherent part and a spin-dependent one. Making the safe assumption that the former one is dominant over the latter, we may write

$$\frac{d\sigma}{dE_R} = \frac{\sigma_0}{E_R^{\text{max}}} F^2(q), \quad (2)$$

where  $\sigma_0$  is the point-like scalar WIMP–nucleus cross section,  $E_R^{\max}$  is the maximum value of  $E_R$  and  $F(q)$  denotes the nuclear form factor, expressed as a function of the momentum transfer  $q^2 \equiv |\vec{q}|^2 = 2m_N E_R$ .  $\sigma_0$  may be conveniently rewritten in terms of the scalar WIMP–nucleon cross section  $\sigma_{\text{scalar}}^{(\text{nucleon})}$

$$\sigma_0 = \left( \frac{1 + m_\chi/m_p}{1 + m_\chi/m_N} \right)^2 A^2 \sigma_{\text{scalar}}^{(\text{nucleon})}, \quad (3)$$

where  $m_p$  is the proton mass and  $A$  is the mass number of the nucleus.

For the nuclear form factor in Eq.(2) we use the Helm parameterization of the scalar form factor [11,12]:

$$F(q) = 3 \frac{j_1(qr_0)}{qr_0} \exp\left(-\frac{1}{2}s^2 q^2\right) \quad (4)$$

where  $s \simeq 1$  fm is the thickness parameter for the nucleus surface,  $r_0 = (r^2 - 5s^2)^{1/2}$ ,  $r = 1.2 A^{1/3}$  fm and  $j_1(qr_0)$  is the spherical Bessel function of index 1.

Once a functional form for  $f(v)$  is chosen and specific values are assigned to the relevant astrophysical velocities, the quantity  $\rho_\chi \sigma_{\text{scalar}}^{(\text{nucleon})}$  may be extracted from measurements of the differential rate  $dR/dE_R$  as a function of  $m_\chi$ .

Here, for  $f(v)$  we take the standard Maxwell–Boltzmann distribution (as in an isothermal spherical model for the halo) with a finite escape velocity, i.e. in the galactic rest frame we write

$$f_{\text{gal}}(v^{\text{gal}}) = N \left( \frac{3}{2\pi v_{\text{rms}}^2} \right)^{3/2} \exp\left(-\frac{3(v^{\text{gal}})^2}{2v_{\text{rms}}^2}\right), \quad (5)$$

where the normalization factor is

$$N = \left[ \text{erf}(z) - \frac{2}{\sqrt{\pi}} z \exp(-z^2) \right]^{-1}, \quad (6)$$

with  $z^2 = 3v_{\text{esc}}^2/(2v_{\text{rms}}^2)$ . In the isothermal spherical model,  $v_{\text{rms}}$  is related to the asymptotic value  $v_\infty$  of the rotational velocities by the relation  $v_{\text{rms}} = \sqrt{\frac{3}{2}}v_\infty$ . The measured rotational velocity remains almost flat (to roughly 15%) between 4 Kpc and 18 Kpc; here, we identify  $v_\infty$  with the rotational velocity of the Local System at the position of the Solar System  $v(r_\odot) \equiv v_0$ , whose physical range will be shortly discussed.

To make use of Eq.(1), Eq.(5) has to be transformed to the rest frame of the Earth, which moves through the Galaxy with a velocity

$$v_\oplus = v_\odot + v_{\text{orb}} \cos \gamma \cos[\omega(t - t_0)], \quad (7)$$

in the azimuthal direction.  $v_\odot$  is given by

$$v_\odot = v_0 + 12 \text{ km s}^{-1}. \quad (8)$$

In these expressions the speed of  $12 \text{ km s}^{-1}$  stands for the motion of the Solar System with respect to the Local System,  $v_{\text{orb}} = 30 \text{ km s}^{-1}$  denotes the Earth orbital speed around the

Sun, the angle  $\gamma \simeq 60^\circ$  is the inclination of the Earth orbital plane with respect to the galactic plane and  $\omega = 2\pi/365\text{days}$ ,  $t_0 = \text{June } 2^{\text{nd}}$  [13,14].

In Refs. [1–3] the DAMA/NaI annual–modulation region was extracted from the experimental data, by using a maximum likelihood method and by taking for the velocities  $v_0$  and  $v_{\text{esc}}$  the following values:  $v_0 = 220 \text{ km s}^{-1}$  and  $v_{\text{esc}} = 650 \text{ km s}^{-1}$  (the relevant region is one of the domains displayed in Fig. 1). The ensuing implications for relic neutralinos, derived in [4–8], refer to the same set of astrophysical velocities.

In the present paper we extend the analysis of the annual–modulation region, by considering the physical ranges associated to  $v_0$  and  $v_{\text{esc}}$  [15–17]:

$$v_0 = (220 \pm 50) \text{ km s}^{-1} \quad (90\% \text{ C.L.}), \quad (9)$$

$$v_{\text{esc}} = (450 \div 650) \text{ km s}^{-1} \quad (90\% \text{ C.L.}). \quad (10)$$

The statistical method for the extraction of the annual–modulation region is the same as the one employed in Refs. [1–3], with a lower bound  $m_\chi \geq 25 \text{ GeV}$ .

On the basis of the analytical properties of the time–modulated part of the detection rate [14], one expects that a variation in  $v_0$  induces a sizeable modification in the range of  $m_\chi$ , without affecting  $\rho_\chi \sigma_{\text{scalar}}^{(\text{nucleon})}$  significantly. Indeed, an increase (decrease) in  $v_0$  is expected to extend the original DAMA/NaI region toward lower (larger) WIMP masses for kinematical reasons;  $\rho_\chi \sigma_{\text{scalar}}^{(\text{nucleon})}$  cannot appreciably change, since it acts as a normalization factor which is determined by the size of the average detection rate. Also, no sizeable variation of both  $m_\chi$  and  $\rho_\chi \sigma_{\text{scalar}}^{(\text{nucleon})}$  is expected from a variation in  $v_{\text{esc}}$ , since the escape velocity provides a cut–off in the integral of Eq.(1) applying only on the flat tail of the velocity distribution  $f(v)$ .

We report in Fig. 1 the ( $2\text{-}\sigma$  C.L.) annual–modulation regions extracted from the DAMA/NaI data of Ref. [3] (total exposure of  $19,511 \text{ kg} \times \text{day}$ ) for sets of values for  $v_0$  and  $v_{\text{esc}}$ , which bracket the ranges given in Eqs.(9–10). The  $1\text{-}\sigma$  ranges for the relevant quantities are given in Table 1. Notice that in Fig. 1 the density  $\rho_\chi$  is given in units of  $0.3 \text{ GeV cm}^{-3}$ , i.e.  $\rho_\chi^{0.3} \equiv \rho_\chi / (0.3 \text{ GeV cm}^{-3})$ .

From the features displayed in Fig. 1 we notice that, as anticipated above: i) the location of the annual–modulation region is rather sensitive to the velocity  $v_0$ , with a sizeable extension in the range of  $m_\chi$ , but with small variations in  $\rho_\chi \sigma_{\text{scalar}}^{(\text{nucleon})}$ ; ii) the annual–modulation region is essentially independent of  $v_{\text{esc}}$ . From the results of Table I we conclude that the uncertainties in  $v_0$  extend the range of  $m_\chi$ , as singled out by the DAMA/NaI annual–modulation data, to (at  $1\text{-}\sigma$  C.L.)

$$30 \text{ GeV} \lesssim m_\chi \lesssim 130 \text{ GeV}. \quad (11)$$

Taking into account the whole ranges of  $v_0$  and  $v_{\text{esc}}$  (see Eqs. (9-10)), we find the annual–modulation region which is depicted in Fig. 2. This region, which envelops the domains displayed in Fig. 1, will be hereafter referred to as region  $R_m$ .

It is worth noticing that this annual–modulation region might be further extended, if a possible bulk rotation of the dark matter halo is introduced. Unfortunately, halo models which take realistically into account this phenomenon are not yet available; however, effects

of rotation of the dark matter halo on direct detection rates and ensuing upper bounds on cross sections have been addressed in some extreme models [18,19]. To obtain an estimate of the effects of a possible rotation of the isothermal sphere one can consider a class of models [20] which describe the fastest rotating steady state by means of the following recipe:

$$f_+(v^{\text{gal}}) = \begin{cases} f(v^{\text{gal}}) & v_\phi^{\text{gal}} > 0 \\ 0 & v_\phi^{\text{gal}} < 0 \end{cases} \quad (12)$$

$$f_-(v^{\text{gal}}) = \begin{cases} 0 & v_\phi^{\text{gal}} > 0 \\ f(v^{\text{gal}}) & v_\phi^{\text{gal}} < 0 \end{cases} \quad (13)$$

where  $v_\phi^{\text{gal}}$  is the azimuthal component of  $\vec{v}$ .

Then one can combine the above functions in order to deal with a more general family of distribution functions  $f_{\text{rot}}(v^{\text{gal}})$ , defined as [18]:

$$f_{\text{rot}}(v^{\text{gal}}) = a f_+(v^{\text{gal}}) + (1 - a) f_-(v^{\text{gal}}), \quad (14)$$

where  $a$  is related to the dimensionless galactic angular momentum parameter  $\lambda$  by the relation  $\lambda = 0.36|a - 0.5|$ . In order to be consistent with the available extensive numerical work on galaxy formation,  $\lambda$  should not exceed the value 0.05 [21].

Adopting the expression in Eq.(14) for the velocity distribution function, one finds that the annual-modulation region may be extended to the domain depicted in Fig. 3, and the relevant range of  $m_\chi$  would become (at  $1-\sigma$  C.L.)

$$30 \text{ GeV} \lesssim m_\chi \lesssim 180 \text{ GeV}. \quad (15)$$

Although the possible occurrence of a bulk rotation of the dark matter halo is a quite interesting possibility deserving further investigation, all subsequent analyses of the present paper will refer to the region  $R_m$ , given in Fig. 2.

### III. SUPERSYMMETRIC MODEL

The WIMP candidate considered in this paper is the neutralino, defined as the lowest-mass linear superposition of photino ( $\tilde{\gamma}$ ), zino ( $\tilde{Z}$ ) and the two higgsino states ( $\tilde{H}_1^\circ$ ,  $\tilde{H}_2^\circ$ ) [22]

$$\chi \equiv a_1 \tilde{\gamma} + a_2 \tilde{Z} + a_3 \tilde{H}_1^\circ + a_4 \tilde{H}_2^\circ. \quad (16)$$

To classify the nature of the neutralino it is useful to define a parameter  $P \equiv a_1^2 + a_2^2$ ; hereafter the neutralino is called a *gaugino*, when  $P > 0.9$ , is called *mixed* when  $0.1 \leq P \leq 0.9$  and a *higgsino* when  $P < 0.1$ .

The theoretical framework adopted here is the Minimal Supersymmetric extension of the Standard Model (MSSM) [22], which conveniently describes the supersymmetric phenomenology at the electroweak scale, without being constrained by too strong theoretical

assumptions. Specific details of the scheme employed in this paper are given in Ref. [6]; here we only recall a few essentials.

The large number of free parameters inherent in the model is reduced to six independent ones, by imposing a few assumptions at the electroweak scale: i) all trilinear parameters are set to zero except those of the third family, which are unified to a common value  $A$ ; ii) all squarks and sleptons soft-mass parameters are taken as degenerate:  $m_{\tilde{t}_i} = m_{\tilde{q}_i} \equiv m_0$ , iii) the gaugino masses are assumed to unify at  $M_{GUT}$ , and this implies that the  $U(1)$  and  $SU(2)$  gaugino masses are related at the electroweak scale by  $M_1 = (5/3) \tan^2 \theta_W M_2$ .

The six independent parameters are taken to be:  $M_2, \mu, \tan \beta, m_A, m_0, A$ , where  $\mu$  is the Higgs-mixing parameter,  $\tan \beta$  is the ratio of the two Higgs vacuum expectation values, and  $m_A$  is the mass of the neutral pseudoscalar Higgs boson. To get the scatter plots shown in this paper, the supersymmetric space has been scanned, by varying the parameters in the following ranges:  $10 \text{ GeV} \leq M_2 \leq 1000 \text{ GeV}$ ,  $10 \text{ GeV} \leq |\mu| \leq 1000 \text{ GeV}$ ,  $80 \text{ GeV} \leq m_A \leq 1 \text{ TeV}$ ,  $100 \text{ GeV} \leq m_0 \leq 1 \text{ TeV}$ ,  $-3 \leq A \leq +3$ ,  $1 \leq \tan \beta \leq 50$ .

Our supersymmetric parameter space is further constrained by all the experimental limits obtained from accelerators on supersymmetric and Higgs searches. The latest data from LEP2 on Higgs, neutralino, chargino and sfermion masses are used [24]. Also the constraints due to the  $b \rightarrow s + \gamma$  process [25,26] have been taken into account (see Ref. [6] for the theoretical details).

The supersymmetric parameter space has also been constrained by the requirement that the neutralino is the Lightest Supersymmetric Particle (LSP), i.e. regions where the gluino or squarks or sleptons are lighter than the neutralino have been excluded.

One further constraint is due to the requirement that the neutralino relic abundance does not exceed the cosmological bound, derivable from measurements of the age of the Universe [27] and of the Hubble constant [28]. We have adopted here a conservative upper bound,  $\Omega_\chi h^2 \leq 0.7$  ( $h$  is the usual Hubble parameter, defined in terms of the present-day value  $H_0$  of the Hubble constant as  $h \equiv H_0 / (100 \text{ km s}^{-1} \text{ Mpc}^{-1})$ ).

The neutralino relic abundance is calculated here as in Ref. [29]. Inclusion of coannihilation effects [30] in the calculation of  $\Omega_\chi h^2$  are not necessary here, since the instances under which these effects might be sizeable are marginal for the supersymmetric configurations concerning the DAMA/NaI data.

Whenever we have to evaluate the neutralino local density, we employ the rescaling procedure. This rescaling consists in assuming that the neutralino local density  $\rho_\chi$  may be taken as  $\rho_\chi = \xi \rho_l$  ( $\rho_l$  is the total local density of non-baryonic dark matter), with  $\xi = \min(1, \Omega_\chi h^2 / (\Omega h^2)_{\min})$ , i.e.,  $\rho_\chi$  may be set equal to  $\rho_l$  only when  $\Omega_\chi h^2$  is larger than a minimal value  $(\Omega h^2)_{\min}$ , compatible with observational data and with large-scale structure calculations; otherwise, when  $\Omega_\chi h^2$  turns out to be less than  $(\Omega h^2)_{\min}$ , and then the neutralino may only provide a fractional contribution  $\Omega_\chi h^2 / (\Omega h^2)_{\min}$  to  $\Omega h^2$ ,  $\rho_\chi$  is reduced by the same fraction  $\xi = \Omega_\chi h^2 / (\Omega h^2)_{\min}$  as compared to  $\rho_l$ . The value to be assigned to  $(\Omega h^2)_{\min}$  is somewhat arbitrary, in the range  $0.01 \lesssim (\Omega h^2)_{\min} \lesssim 0.2$ . In the present paper, whenever we have to apply rescaling, we use the value  $(\Omega h^2)_{\min} = 0.01$ , which is conservatively derived from the estimate  $\Omega_{\text{galactic}} \sim 0.03$ .

In Fig. 2 we display our results for  $\rho_\chi^{0.3} \sigma_{\text{scalar}}^{(\text{nucleon})}$  in the form of the scatter plot which is derived by scanning the supersymmetric parameter space over the grid defined above. For

the evaluation of  $\sigma_{\text{scalar}}^{(\text{nucleon})}$  we use the expressions given in Ref. [6]. We notice that a host of configurations fall inside the region  $R_m$ ; thus, the annual-modulation region is compatible with supersymmetric configurations currently allowed by accelerator constraints.

#### IV. INTERPRETATION OF THE ANNUAL-MODULATION DATA IN TERMS OF RELIC NEUTRALINOS

Let us turn now to the implications of the DAMA/NaI experimental data, once these are interpreted in terms of relic neutralinos. The cosmological properties are examined first; other prominent features of the relevant supersymmetric configurations will be examined afterwards.

##### A. Neutralino cosmological properties

For the derivation of the relic neutralino properties as regards its local density  $\rho_\chi$  as well as its contribution to the average relic abundance  $\Omega_\chi h^2$  compatible with region  $R_m$ , we adopt the straightforward procedure, outlined in Ref. [5], which does not require any use of rescaling in the local neutralino density. The method is the following:

1) We evaluate  $\sigma_{\text{scalar}}^{(\text{nucleon})}$  and  $\Omega_\chi h^2$  by varying the supersymmetric parameters over the grid and with the constraints defined in the previous section.

2) For any value of  $[\rho_\chi \sigma_{\text{scalar}}^{(\text{nucleon})}]_{\text{expt}}$  compatible with the region  $R_m$  we calculate  $\rho_\chi$  as given by  $\rho_\chi = [\rho_\chi \sigma_{\text{scalar}}^{(\text{nucleon})}]_{\text{expt}} / \sigma_{\text{scalar}}^{(\text{nucleon})}$  and restrict the values of  $m_\chi$  to stay inside the region  $R_m$  displayed in Fig. 2.

3) The results are then displayed in a scatter plot in the plane  $\rho_\chi$  vs.  $\Omega_\chi h^2$ .

Examples of our results are given in Figs. 4 a–c for a few experimentally allowed values of  $\rho_\chi \sigma_{\text{scalar}}^{(\text{nucleon})}$ , which bracket the range implied by the region  $R_m$  of Fig. 2. Sects. a–c of Figs. 4 refer to the values  $[\rho_\chi \sigma_{\text{scalar}}^{(\text{nucleon})}]_{\text{expt}} = 4 \cdot 10^{-9}$  nbarn,  $6 \cdot 10^{-9}$  nbarn and  $8 \cdot 10^{-9}$  nbarn, respectively.

The two horizontal lines delimit the physical range  $0.1 \text{ GeV cm}^{-3} \leq \rho_l \leq 0.7 \text{ GeV cm}^{-3}$  for the total local density of non-baryonic dark matter. This (rather generous) range has been established by taking into account a possible flattening of the dark matter halo [31,32] and a possibly sizeable baryonic contribution to the galactic dark matter [33]. The solid vertical lines delimit the cosmologically interesting the range  $0.01 \leq \Omega_\chi h^2 \leq 0.7$ . The two vertical dashed lines delimit the range:  $0.02 \leq \Omega_\chi h^2 \leq 0.2$ , which represents the most appealing interval. Indeed, recent observations and analyses [34] favour  $0.1 \lesssim \Omega_{\text{matter}} \lesssim 0.4$ . Combining this range with the one for  $h$ :  $0.55 \lesssim h \lesssim 0.80$  [28] and requiring that a cold dark matter candidate (such as the neutralino) supplies  $\sim (80\text{--}90)\%$  of  $\Omega_{\text{matter}}$ , we actually obtain:  $0.02 \lesssim \Omega_{\text{CDM}} h^2 \lesssim 0.2$ .

The two slant dot-dashed lines delimit the band where linear rescaling procedure for the local density is usually applied. In Figs. 4 a–c the upper dot-dashed line would refer to a rescaling with  $(\Omega h^2)_{\text{min}} = 0.01$ , the lower one to the value  $(\Omega h^2)_{\text{min}} = 0.2$ . However, notice that *in the derivation of the scatter plot of Figs. 4 a–c, no use of rescaling for  $\rho_\chi$  is made.*



With the aid of this kind of plot we can classify the supersymmetric configurations belonging to region  $R_m$  into various categories. Configurations whose representative points fall above the maximum value  $\rho_\chi = 0.7 \text{ GeV cm}^{-3}$  have to be excluded (we remind that those providing an  $\Omega_\chi h^2 > 0.7$  are already disregarded from the very beginning). Among the allowed configurations, those falling in the region inside both the horizontal and solid vertical lines (called  $A$  hereafter) are very appealing, since they would represent situations where the neutralino could have the role of a dominant cold dark matter component; even more so, if the representative points fall in the subregion (called  $B$  hereafter) inside the vertical band delimited by dashed lines. Configurations which fall inside the band delimited by the slant dot–dashed lines denote situations where the neutralino can only provide a fraction of the cold dark matter both at the level of local density and at the level of the average  $\Omega$ . Configurations above the upper dot–dashed line and below the upper horizontal solid line would imply a stronger clustering of neutralinos in our halo as compared to their average distribution in the Universe.

It is worth noticing a few important properties of the scatter plots shown in Figs. 4 a–c:

- 1) The scatter plots display a correlation between  $\rho_\chi$  and  $\Omega_\chi h^2$ . This feature is expected on the basis of the following properties: i)  $\Omega_\chi h^2$  is roughly inversely proportional to the neutralino pair annihilation cross section, ii) at fixed  $[\rho_\chi \sigma_{\text{scalar}}^{(\text{nucleon})}]_{\text{expt}}$ ,  $\rho_\chi$  is inversely proportional to  $\sigma_{\text{scalar}}^{(\text{nucleon})}$ , iii) the annihilation cross section and  $\sigma_{\text{scalar}}^{(\text{nucleon})}$  are usually correlated functions (i.e., they are both increasing or decreasing functions of the supersymmetric parameters).
- 2) The domains covered by the supersymmetric configurations in regions  $A$  and  $B$  are slightly larger for smaller values of  $[\rho_\chi \sigma_{\text{scalar}}^{(\text{nucleon})}]_{\text{expt}}$ . This feature follows from the fact that  $\sigma_{\text{scalar}}^{(\text{nucleon})}$  is bounded from above by accelerator limits (mainly because of lower bounds on Higgs masses); this implies for  $\rho_\chi$  a lower bound, which however is less stringent at lower values of  $[\rho_\chi \sigma_{\text{scalar}}^{(\text{nucleon})}]_{\text{expt}}$ .

We can conclude that the DAMA/NaI data are compatible with a relic neutralino as a major component of dark matter in the universe.

## B. Other properties of the supersymmetric configurations of set $S_m$

Apart from the cosmological properties previously discussed, one of the most interesting questions is whether the supersymmetric configurations, whose representative points fall inside the region  $R_m$  of Fig. 2 (hereafter denoted as configurations of set  $S_m$ ), are explorable at accelerators of the present generation. This point was investigated in Ref. [6] in the case of the original DAMA/NaI annual–modulation region. Here we extend our considerations to the larger set  $S_m$  derived from region  $R_m$ .

The supersymmetric configurations of set  $S_m$  are constrained by the inequalities

$$\frac{[\rho_\chi \sigma_{\text{scalar}}^{(\text{nucleon})}]_{\text{expt}}}{\rho_{\chi,\text{max}}} \leq \sigma_{\text{scalar}}^{(\text{nucleon})} \leq \frac{[\rho_\chi \sigma_{\text{scalar}}^{(\text{nucleon})}]_{\text{expt}}}{\rho_{\chi,\text{min}}} \quad (17)$$

where  $\rho_{\chi,\min} = \xi\rho_{l,\min} = \xi \cdot 0.1 \text{ GeV cm}^{-3}$  and  $\rho_{\chi,\max} = \xi\rho_{l,\max} = \xi \cdot 0.7 \text{ GeV cm}^{-3}$ , and  $[\rho_{\chi}\sigma_{\text{scalar}}^{(\text{nucleon})}]_{\text{expt}}$  is any value inside region  $R_m$  as a function of  $m_{\chi}$ .

Eq.(17) implies interesting correlations among the supersymmetric parameters, as displayed in Figs. 5–7. The first of these figures shows the scatter plot of  $\tan\beta$  versus the mass  $m_h$  of the lightest neutral CP-even Higgs boson (we recall that  $m_h$  may be derived from the supersymmetric parameters listed in Sect. III). The correlation displayed in Fig. 5 between  $\tan\beta$  and  $m_h$  is implied by the fact that  $\sigma_{\text{scalar}}^{(\text{nucleon})}$  is usually dominated by Higgs-exchange amplitudes, and these are in turn large for large values of  $\tan\beta$  and small values of  $m_h$ . As is apparent in Fig. 5 a number of supersymmetric configurations of set  $S_m$  could still be explorable at LEP2, but the others require investigation at a high luminosity Fermilab Tevatron [35,36] or at LHC. Fig. 6 shows a correlation between  $\tan\beta$  and the mass of the lightest top–squark  $m_{\tilde{t}_1}$ . The reasons for this feature are more involved, and are discussed in Ref. [6].

A last plot, providing  $\tan\beta$  versus  $m_{\chi}$ , is given in Fig. 7. Again, a correlation shows up here for not too large values of  $\tan\beta$ . LEP2 can only provide an investigation up to  $m_{\chi} \simeq 50 \text{ GeV}$ . The exploration up to  $\sim 125 \text{ GeV}$  can be performed with Tevatron upgrades (under favorable conditions), while for higher values of  $m_{\chi}$  LHC is needed.

## V. CONCLUSIONS

We have investigated how the original DAMA/NaI annual–modulation region in the plane  $\rho_{\chi}\sigma_{\text{scalar}}^{(\text{nucleon})} - m_{\chi}$  is extended when the uncertainties in the galactic astrophysical velocities are taken into account. One of the most noticeable consequences is that the range for the neutralino mass becomes  $30 \text{ GeV} \lesssim m_{\chi} \lesssim 130 \text{ GeV}$  at  $1\text{-}\sigma$  C.L., with a further extension in the upper bound, when a possible bulk rotation of the dark matter halo is taken into account. However, the extension of the modulation region implies only slight modifications in the correlations among the supersymmetric parameters in the MSSM scheme.

We have found that a number of supersymmetric configurations singled out by the DAMA/NaI results have cosmological properties compatible with a relic neutralino as a dominant component of cold dark matter (on the average in our universe and in our galactic halo). It has also been discussed the discovery potential for the relevant supersymmetric configurations at accelerators of present generation.

## Acknowledgments

A.B., F.D. and N.F. are grateful to Venya Berezhinsky for interesting discussions about halo bulk rotations. This work was supported by DGICYT under grant number PB95–1077 and by the TMR network grant ERBFMRXCT960090 of the European Union.

## Note added

During the completion of this work there appeared two preprints: hep-ph/9903467 (by L. Roszkowski) and hep-ph/9903468 (by M. Brhlik and L. Roszkowski), where some considerations on the effect of astrophysical velocities uncertainty on WIMP direct searches are presented.

## REFERENCES

- [1] R. Bernabei *et al.*, Phys. Lett. B **424**, 195 (1998).
- [2] R. Bernabei *et al.*, University of Rome Report No. ROM2F/98/27 (submitted for publication).
- [3] R. Bernabei *et al.*, University of Rome Report No. ROM2F/98/34 and INFN Report No. INFN/AE-98/20 (to appear in Phys. Lett. B).
- [4] A. Bottino, F. Donato, N. Fornengo and S. Scopel, Phys. Lett. B **423**, 109 (1998).
- [5] A. Bottino, F. Donato, N. Fornengo and S. Scopel, *hep-ph/9710295*, Torino University Report No. DFTT 61/97 (unpublished).
- [6] A. Bottino, F. Donato, N. Fornengo and S. Scopel, *hep-ph/9808456*, Torino University Report No. DFTT 41/98 (to appear in Phys. Rev. D).
- [7] A. Bottino, F. Donato, N. Fornengo and S. Scopel, *hep-ph/9808459*, Torino University Report No. DFTT 48/98 (to appear in Phys. Rev. D).
- [8] A. Bottino, F. Donato, N. Fornengo and S. Scopel, Astropart. Phys. **10**, 203 (1999).
- [9] For an analysis of the DAMA/NaI annual-modulation data in supergravity unified models, see also R. Arnowitt and P. Nath, *hep-ph/9902237*.
- [10] For preliminary results of our analysis see: N. Fornengo, *hep-ph/9812210*, *Proceeding of the International Workshop on the Identification of Dark Matter (IDM98), Buxton, 1998*, edited by N. Spooner (World Scientific, to appear); R. Bernabei and A. Bottino, talks given at the VIII International Workshop on Neutrino Telescopes (Venice, February 1999); transparencies available at <http://axpd24.pd.infn.it/conference/venice99.html>.
- [11] R.H. Helm, Phys. Rev. D **104**, 1466 (1956).
- [12] J. Engel, Phys. Lett. B **264**, 114 (1991).
- [13] A.K. Drukier, K. Freese and D.N. Spergel, Phys. Rev. D **33**, 3495 (1986).
- [14] K. Freese, J. Frieman and A. Gould, Phys. Rev. D **37**, 3388 (1988).
- [15] P.J.T. Leonard and S. Tremaine, Astrophys. J. **353**, 486 (1990).
- [16] C.S. Kochanek, Astrophys. J. **457**, 228 (1996).
- [17] K.M. Cudworth, Astron. J. **99**, 590 (1990).
- [18] M. Kamionkowski and A. Kinkhabwala, Phys. Rev. D **57**, 3256 (1998).
- [19] F. Donato, N. Fornengo and S. Scopel, Astropart. Phys. **9**, 297 (1998).
- [20] D. Lynden-Bell, Mon. Not. R. Astron. Soc. **120**, 204 (1960).
- [21] S. Warren, P.J. Quinn, J.K. Salmon, W.H. Zurek, Astrophys. J. **399**, 405 (1992); S. Cole, C. Lacey, Mon. Not. R. Astron. Soc. **281**, 716 (1996).
- [22] H.P. Nilles, Phys. Rep. **110**, 1 (1984); H.E. Haber and G.L. Kane, Phys. Rep. **117**, 75 (1985); R. Barbieri, Riv. Nuovo Cim. **11**, 1 (1988).
- [23] V. Berezhinsky, A. Bottino, J. Ellis, N. Fornengo, G. Mignola and S. Scopel, Astropart. Phys. **5**, 1 (1996).
- [24] V. Ruhlmann-Kleider (DELPHI Collaboration), presentation at the LEPC Conference, November 1998; R. Clare (L3 Collaboration), *ibid.*
- [25] S. Glenn (CLEO Collaboration), Report No. CLEO CONF 98-17, 1998, Proceedings of the International Conference on High Energy Physics, Vancouver, 1998, paper 1011.
- [26] R. Barate *et al.* (ALEPH Collaboration), CERN Report No. CERN-EP/98-044, 1998.
- [27] B. Chaboyer, P. Demarque, P. Kernan and L.M. Krauss, Astrophys. J. **494**, 96 (1998).

- [28] A. Sandage *et al.*, *Astrophys. J. Lett.* **460**, L15 (1996); W. L. Freedman, *astro-ph/9706072*, *Proceedings of the 18th Texas Symposium on Relativistic Astrophysics*, edited by A. Olinto, J. Frieman and D. Schramm (World Scientific, to appear). and references quoted therein.
- [29] A. Bottino, V. de Alfaro, N. Fornengo, G. Mignola and M. Pignone, *Astropart. Phys.* **2**, 67 (1994).
- [30] P. Binétruy, G. Girardi and P. Salati, *Nucl. Phys.* **B237**, 285 (1984); K. Griest and D. Seckel, *Phys. Rev.* **D43**, 3191 (1991); S. Mizuta and M. Yamaguchi, *Phys. Lett.* **B298**, 120 (1993); J. Edsjö and P. Gondolo, *Phys. Rev.* **D56**, 1879 (1997).
- [31] E. Gates, G. Gyuk and M.S. Turner, *Phys. Rev. Lett.* **74**, 3724 (1995); *Phys. Rev.* **D53**, 4138 (1996).
- [32] E. Gates, G. Gyuk and M.S. Turner, *Astrophys. J. Lett.* **449**, L123 (1995).
- [33] E. Gates, G. Gyuk and M.S. Turner, *astro-ph/9704253*, *Proceedings of the 18th Texas Symposium on Relativistic Astrophysics*, edited by A. Olinto, J. Frieman and D. Schramm (World Scientific, to appear).
- [34] W.L. Freedman, R. Kirshner and C. Lineweaver, talks given at the International Conference of Cosmology and Particle Physics (CAPP98), CERN, June 1998, [wwwth.cern.ch/capp98/programme.html](http://wwwth.cern.ch/capp98/programme.html); M. White, *Astrophys. J.* **506**, 495 (1998); N.A. Bahcall and X. Fan, *astro-ph/9804082* to appear in *National Academy of Sciences Proc.*; C. Lineweaver, *astro-ph/9805326*, (to appear in *Astrophys. J. Lett.*).
- [35] Report of the TeV–2000 Study Group, edited by D. Amidei, R. Brock, Fermilab Report No. FERMILAB–PUB–96/082, 1996.
- [36] H. Baer, B.W. Harris and X. Tata, Florida State University *Phys. Rev. D* **59** 015003 (1999).

## TABLES

TABLE I. Results of the maximum likelihood method when varying the velocity parameters ( $v_0$  and  $v_{\text{esc}}$ ) of the WIMP velocity distribution. The values of  $m_\chi$  and  $\sigma_{\text{scalar}}^{(\text{nucleon})}$  correspond to the minima of the maximum likelihood method (with  $1\text{-}\sigma$  error bars).

$v_0$ (km/s)	$v_{\text{esc}}$ (km/s)	$m_\chi$ (GeV)	$\sigma_{\text{scalar}}^{(\text{nucleon})}$ ( $10^{-9}$ nbarn)
220	450	$59^{+17}_{-11}$	$(7.3^{+0.5}_{-1.2})$
220	550	$59^{+16}_{-13}$	$(7.0^{+0.5}_{-1.2})$
220	650	$59^{+17}_{-14}$	$(7.0^{+0.4}_{-1.2})$
170	550	$95^{+29}_{-20}$	$(8.3^{+0.5}_{-1.2})$
270	550	$41^{+14}_{-7}$	$(6.8^{+0.4}_{-1.3})$

## FIGURES

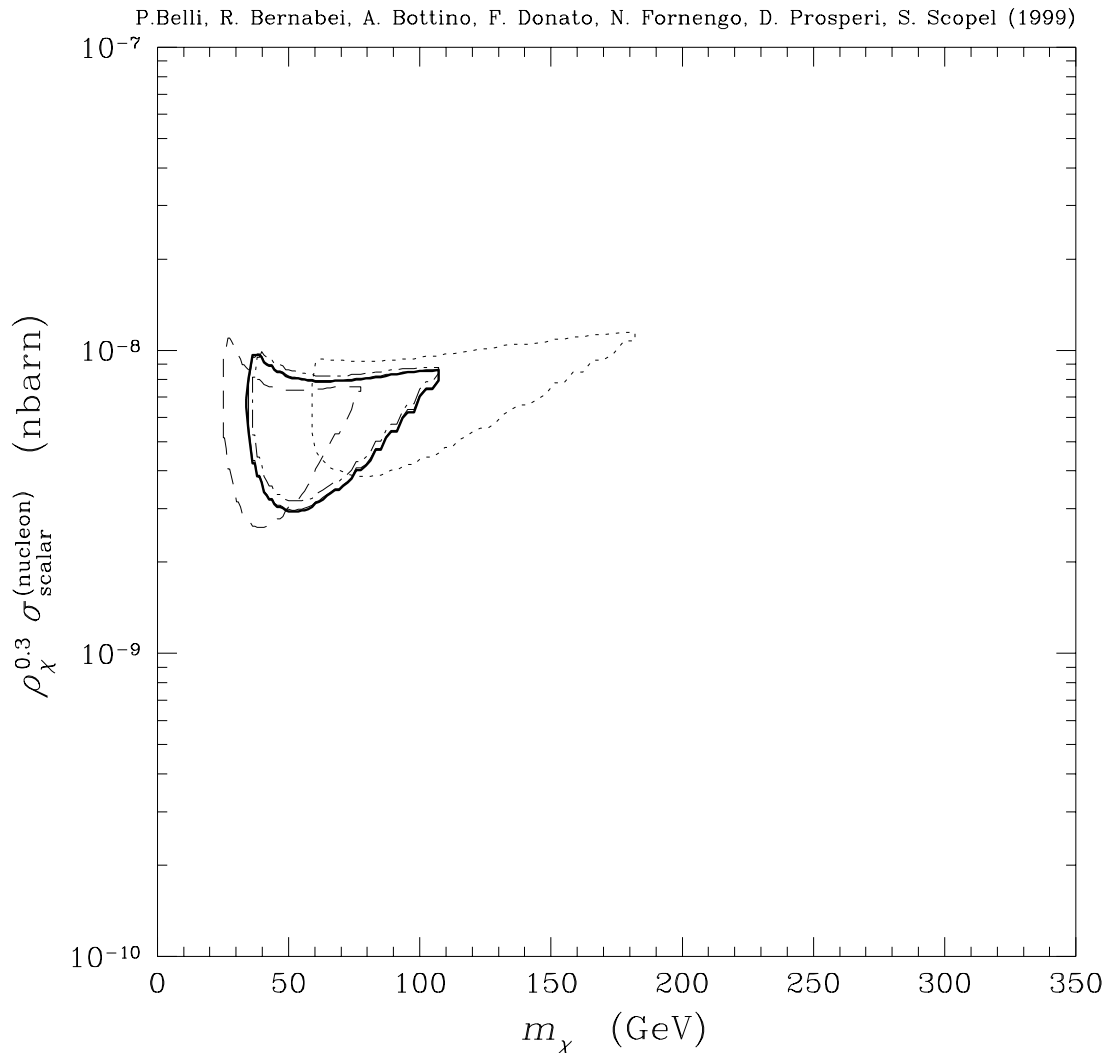


FIG. 1. Annual-modulation regions singled out by the DAMA/NaI experiment [3] in the plane  $\rho_\chi^{0.3} \sigma_{\text{scalar}}^{(\text{nucleon})} - m_\chi$  for various values of velocities  $v_0$  and  $v_{esc}$ :  $v_0 = 220 \text{ km s}^{-1}$ ,  $v_{esc} = 650 \text{ km s}^{-1}$  (solid line);  $v_0 = 220 \text{ km s}^{-1}$ ,  $v_{esc} = 450 \text{ km s}^{-1}$  (dot-dashed line);  $v_0 = 170 \text{ km s}^{-1}$ ,  $v_{esc} = 550 \text{ km s}^{-1}$  (dotted line);  $v_0 = 270 \text{ km s}^{-1}$ ,  $v_{esc} = 550 \text{ km s}^{-1}$  (dashed line). The countour line for  $v_0 = 220 \text{ km s}^{-1}$ ,  $v_{esc} = 550 \text{ km s}^{-1}$  is undistinguishable on the plot from the solid line. The quantity  $\rho_\chi^{0.3}$  is the local neutralino matter density in units of  $0.3 \text{ GeV cm}^{-3}$ , i.e.  $\rho_\chi^{0.3}/(0.3 \text{ GeV cm}^{-3})$ .

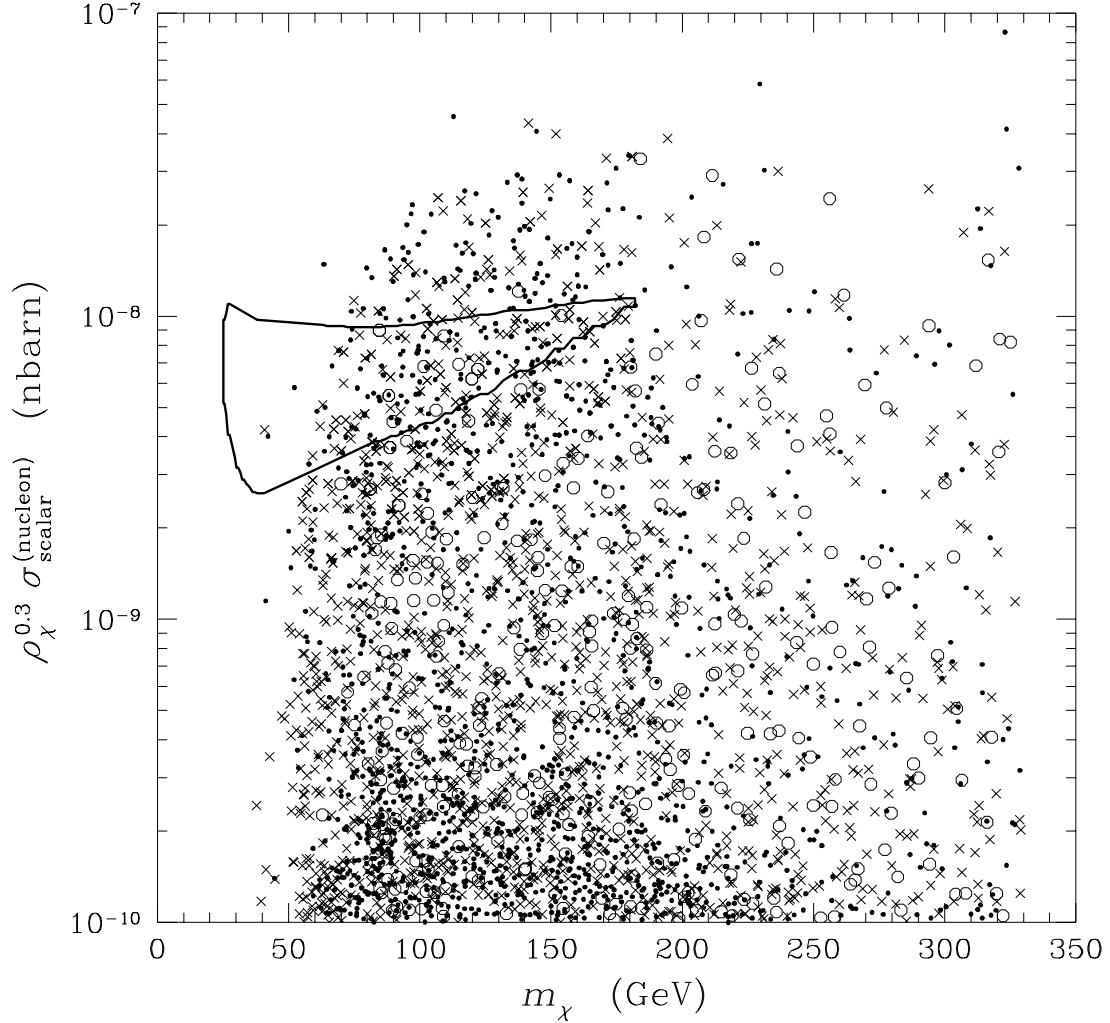


FIG. 2. The contour line delimits the annual-modulation region obtained by varying the velocities  $v_0$  and  $v_{esc}$  over the ranges given in Eqs. (9 – 10). The scatter plot represents the theoretical predictions of a generic MSSM, as described in Sect. III. Different symbols identify different neutralino compositions: circles stand for a higgsino, crosses for a gaugino and dots for a mixed neutralino.

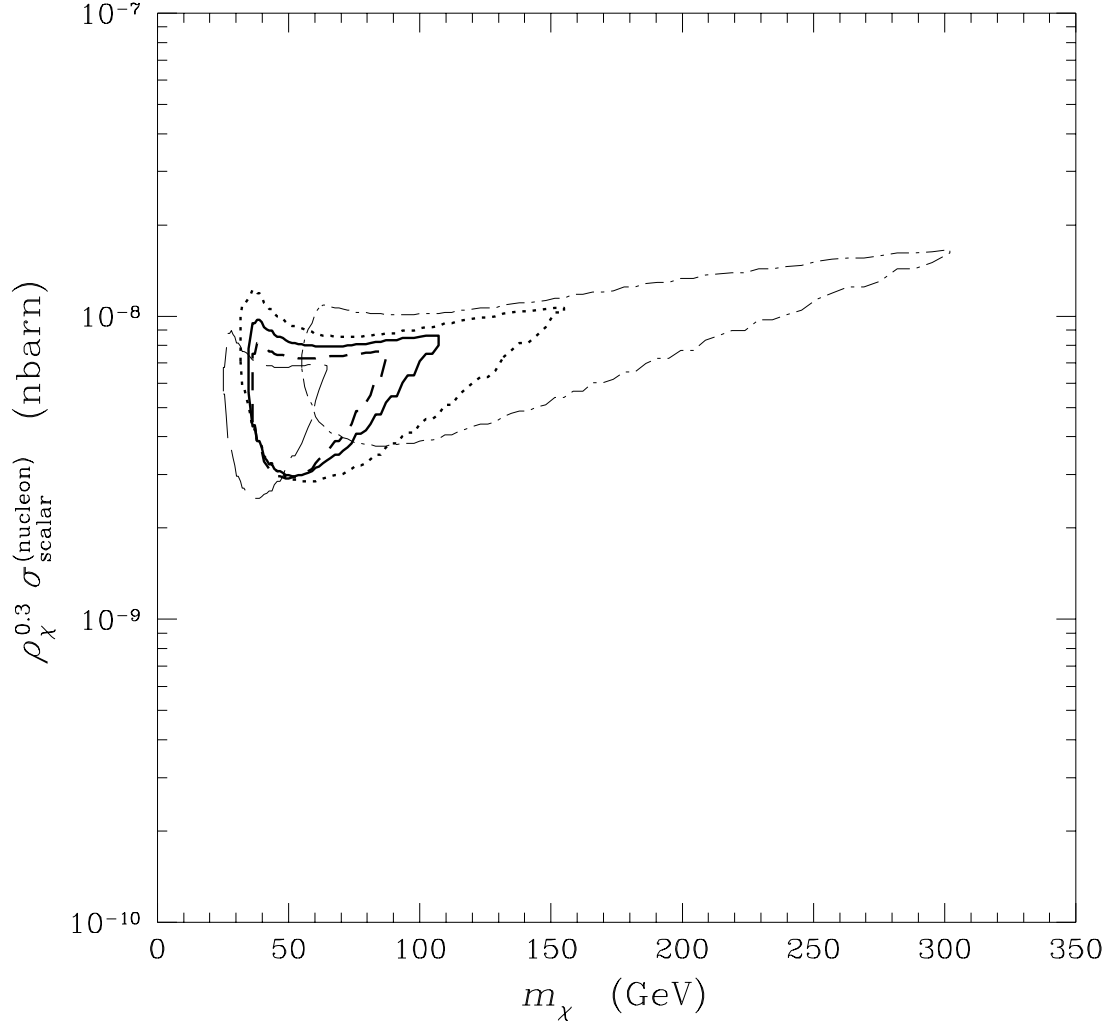


FIG. 3. Annual-modulation regions when a possible bulk rotation of the dark matter halo is taken into account. The contour lines refer to the following halo parameters:  $v_0 = 220$  km s $^{-1}$ , non rotating halo (solid line);  $v_0 = 220$  km s $^{-1}$ , co-rotating halo with spin parameter  $\lambda = 0.05$  (dotted line);  $v_0 = 220$  km s $^{-1}$ , counter-rotating halo with  $\lambda = 0.05$  (dashed line);  $v_0 = 170$  km s $^{-1}$ , co-rotating halo with  $\lambda = 0.05$  (dot-dashed line);  $v_0 = 270$  km s $^{-1}$ , counter-rotating halo with  $\lambda = 0.05$  (long-dashed line); The escape velocity is fixed at the value  $v_{esc} = 550$  km s $^{-1}$  for all the contours.



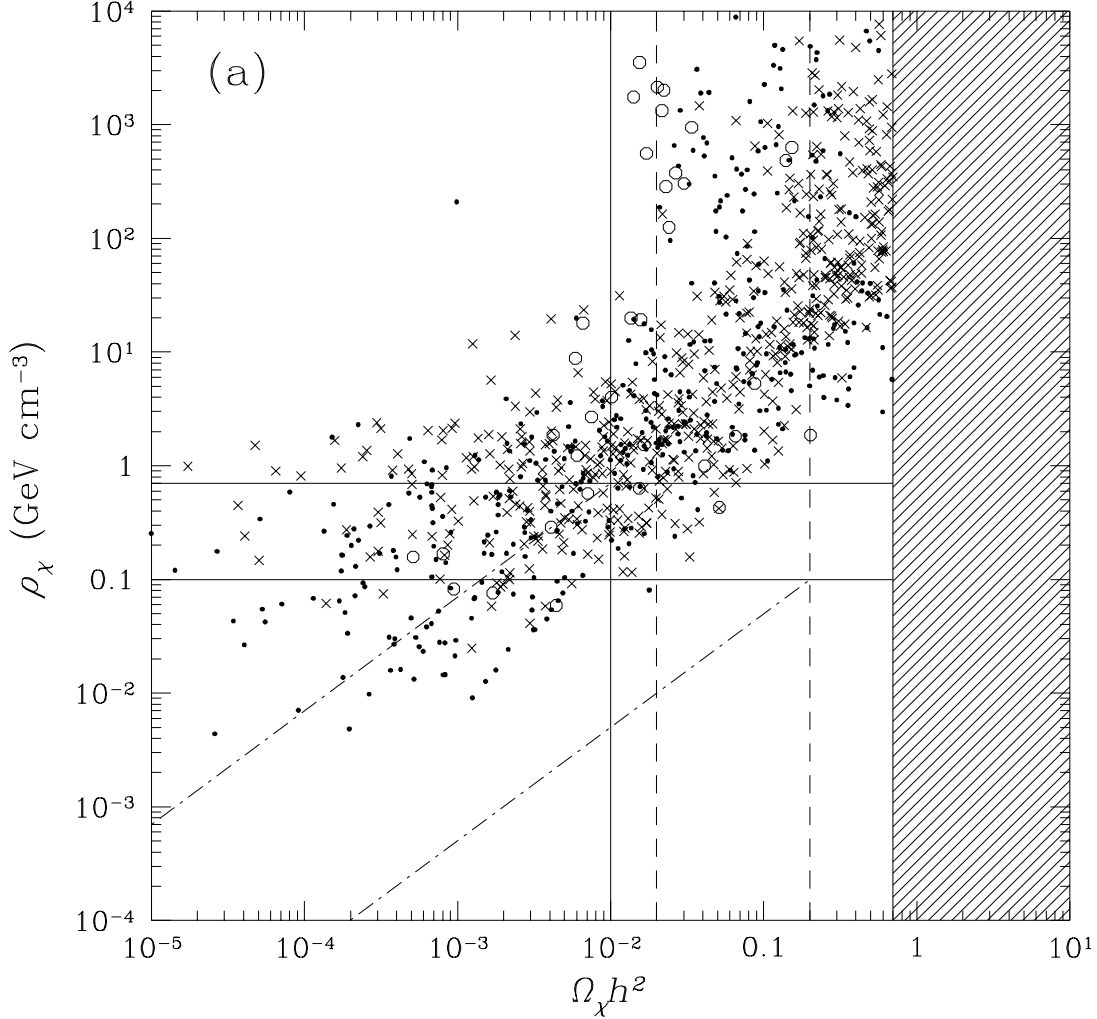


FIG. 4a. The neutralino local density  $\rho_\chi$ , calculated for fixed values of  $[\rho_\chi^{0.3} \sigma_{\text{scalar}}^{\text{nucleon}}]_{\text{expt}}$ , is plotted versus the neutralino relic abundance  $\Omega_\chi h^2$ . For any value of  $[\rho_\chi^{0.3} \sigma_{\text{scalar}}^{\text{nucleon}}]_{\text{expt}}$  the neutralino mass is restricted to the range dictated by the contour line of Fig. 2. The different panels of the figure correspond to the following choices: (a)  $[\rho_\chi^{0.3} \sigma_{\text{scalar}}^{\text{nucleon}}]_{\text{expt}} = 4 \cdot 10^{-9}$  nbarn and  $28 \text{ GeV} \leq m_\chi \leq 88 \text{ GeV}$ ; (b)  $[\rho_\chi^{0.3} \sigma_{\text{scalar}}^{\text{nucleon}}]_{\text{expt}} = 6 \cdot 10^{-9}$  nbarn and  $25 \text{ GeV} \leq m_\chi \leq 131 \text{ GeV}$ ; (c)  $[\rho_\chi^{0.3} \sigma_{\text{scalar}}^{\text{nucleon}}]_{\text{expt}} = 8 \cdot 10^{-9}$  nbarn and  $25 \text{ GeV} \leq m_\chi \leq 156 \text{ GeV}$ . The two horizontal lines delimit the physical range for the local density for non-baryonic dark matter. The two solid vertical lines delimit the interval of  $\Omega_\chi h^2$  of cosmological interest. The two vertical dashed lines delimit the preferred band for cold dark matter. The two slant dot-dashed lines delimit the band where linear rescaling procedure is usually applied.

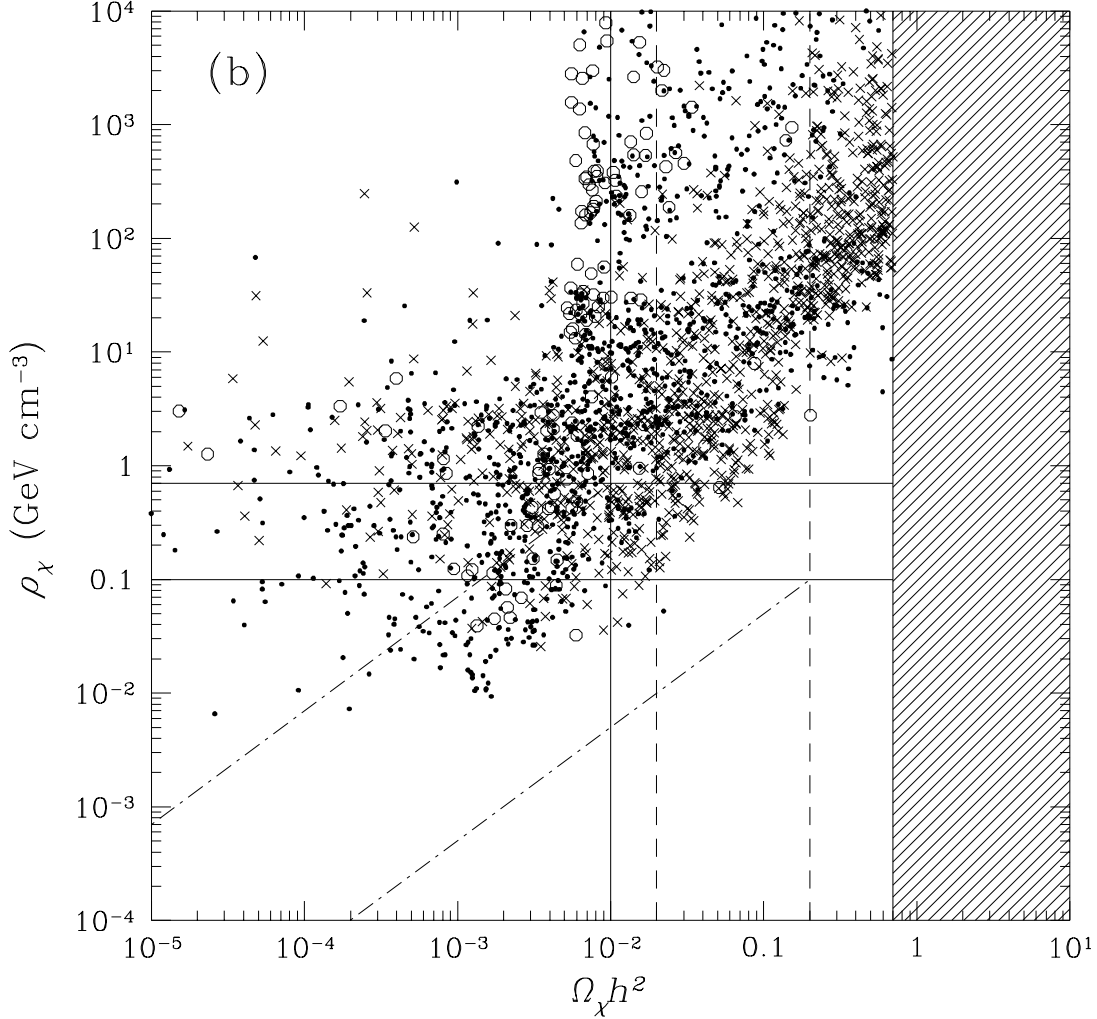


FIG. 4b. The neutralino local density  $\rho_\chi$ , calculated for fixed values of  $[\rho_\chi^{0.3} \sigma_{\text{scalar}}^{\text{nucleon}}]_{\text{expt}}$ , is plotted versus the neutralino relic abundance  $\Omega_\chi h^2$ . For any value of  $[\rho_\chi^{0.3} \sigma_{\text{scalar}}^{\text{nucleon}}]_{\text{expt}}$  the neutralino mass is restricted to the range dictated by the contour line of Fig. 2. The different panels of the figure correspond to the following choices: (a)  $[\rho_\chi^{0.3} \sigma_{\text{scalar}}^{\text{nucleon}}]_{\text{expt}} = 4 \cdot 10^{-9}$  nbarn and  $28 \text{ GeV} \leq m_\chi \leq 88 \text{ GeV}$ ; (b)  $[\rho_\chi^{0.3} \sigma_{\text{scalar}}^{\text{nucleon}}]_{\text{expt}} = 6 \cdot 10^{-9}$  nbarn and  $25 \text{ GeV} \leq m_\chi \leq 131 \text{ GeV}$ ; (c)  $[\rho_\chi^{0.3} \sigma_{\text{scalar}}^{\text{nucleon}}]_{\text{expt}} = 8 \cdot 10^{-9}$  nbarn and  $25 \text{ GeV} \leq m_\chi \leq 156 \text{ GeV}$ . The two horizontal lines delimit the physical range for the local density for non-baryonic dark matter. The two solid vertical lines delimit the interval of  $\Omega_\chi h^2$  of cosmological interest. The two vertical dashed lines delimit the preferred band for cold dark matter. The two slant dot-dashed lines delimit the band where linear rescaling procedure is usually applied.

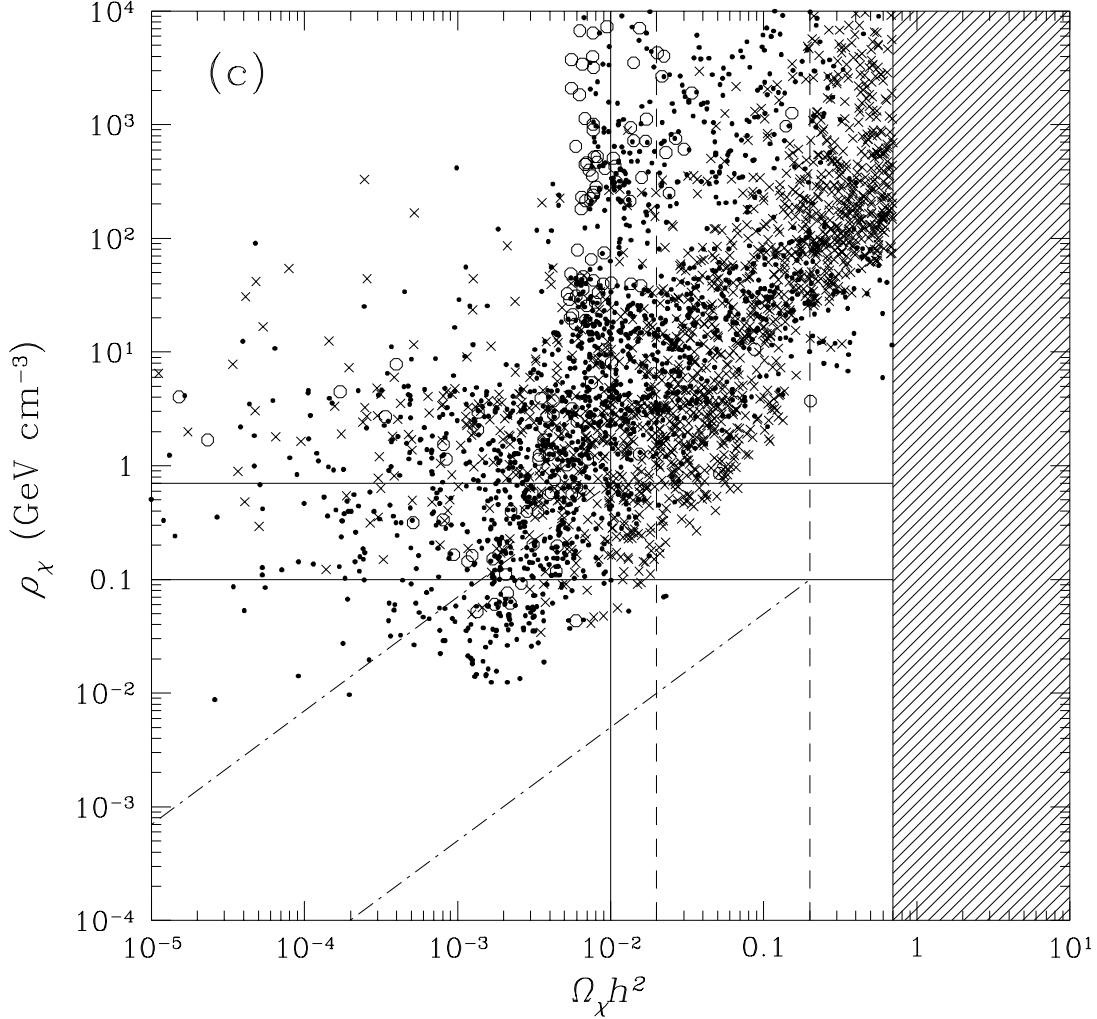


FIG. 4c. The neutralino local density  $\rho_\chi$ , calculated for fixed values of  $[\rho_\chi^{0.3} \sigma_{\text{scalar}}^{\text{nucleon}}]_{\text{expt}}$ , is plotted versus the neutralino relic abundance  $\Omega_\chi h^2$ . For any value of  $[\rho_\chi^{0.3} \sigma_{\text{scalar}}^{\text{nucleon}}]_{\text{expt}}$  the neutralino mass is restricted to the range dictated by the contour line of Fig. 2. The different panels of the figure correspond to the following choices: (a)  $[\rho_\chi^{0.3} \sigma_{\text{scalar}}^{\text{nucleon}}]_{\text{expt}} = 4 \cdot 10^{-9}$  nbarn and  $28 \text{ GeV} \leq m_\chi \leq 88 \text{ GeV}$ ; (b)  $[\rho_\chi^{0.3} \sigma_{\text{scalar}}^{\text{nucleon}}]_{\text{expt}} = 6 \cdot 10^{-9}$  nbarn and  $25 \text{ GeV} \leq m_\chi \leq 131 \text{ GeV}$ ; (c)  $[\rho_\chi^{0.3} \sigma_{\text{scalar}}^{\text{nucleon}}]_{\text{expt}} = 8 \cdot 10^{-9}$  nbarn and  $25 \text{ GeV} \leq m_\chi \leq 156 \text{ GeV}$ . The two horizontal lines delimit the physical range for the local density for non-baryonic dark matter. The two solid vertical lines delimit the interval of  $\Omega_\chi h^2$  of cosmological interest. The two vertical dashed lines delimit the preferred band for cold dark matter. The two slant dot-dashed lines delimit the band where linear rescaling procedure is usually applied.

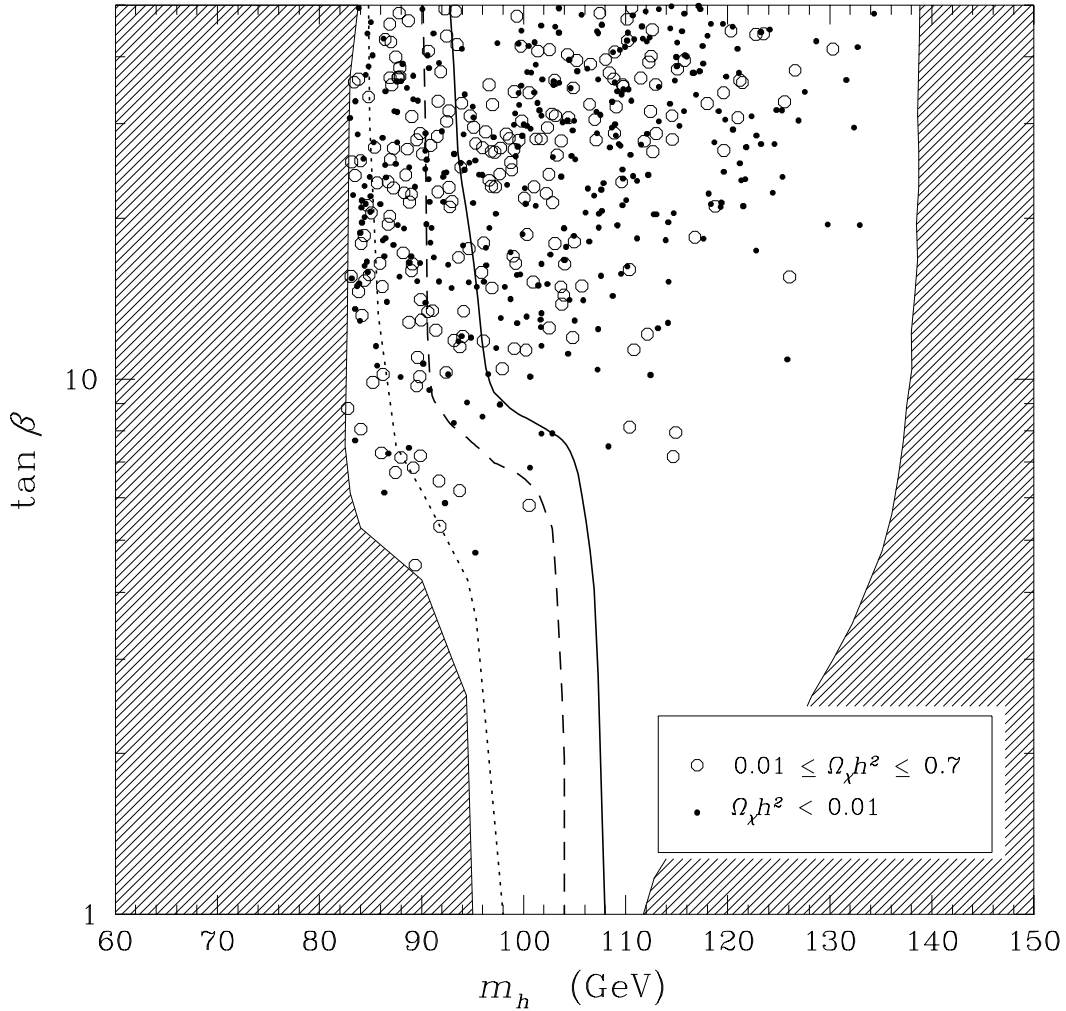


FIG. 5. Scatter plot for set  $S$  in the plane  $m_h - \tan \beta$ . The hatched region on the right is excluded by theory. The hatched region on the left is excluded by present LEP data at  $\sqrt{s} = 189$  GeV. The dotted and the dashed curves denote the reach of LEP2 at energies  $\sqrt{s} = 192$  GeV and  $\sqrt{s} = 200$  GeV, respectively. The solid line represents the 95% C.L. bound reachable at LEP2, in case of non discovery of a neutral Higgs boson.

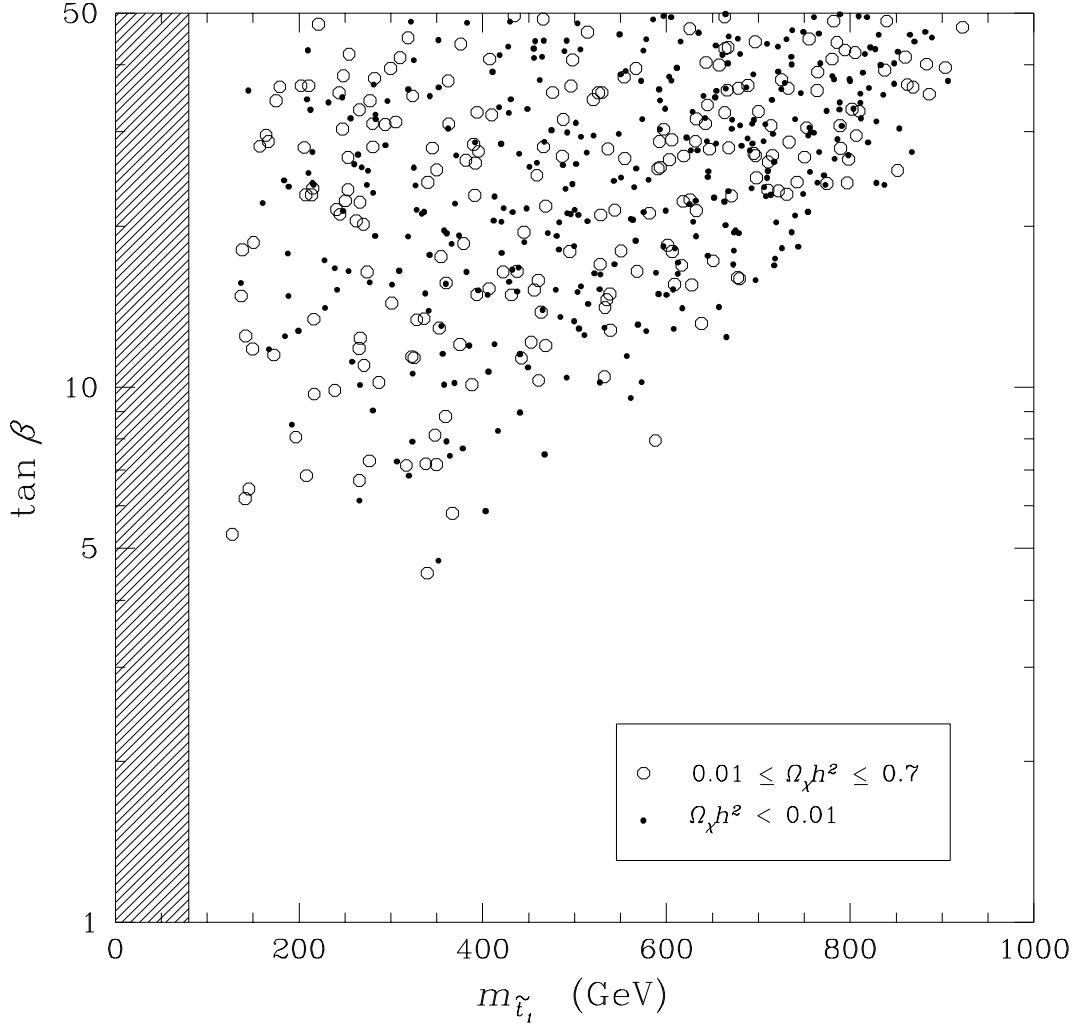


FIG. 6. Scatter plot for set  $S$  in the plane  $m_{\tilde{\tau}_1} - \tan \beta$ . The hatched region is excluded by LEP data.

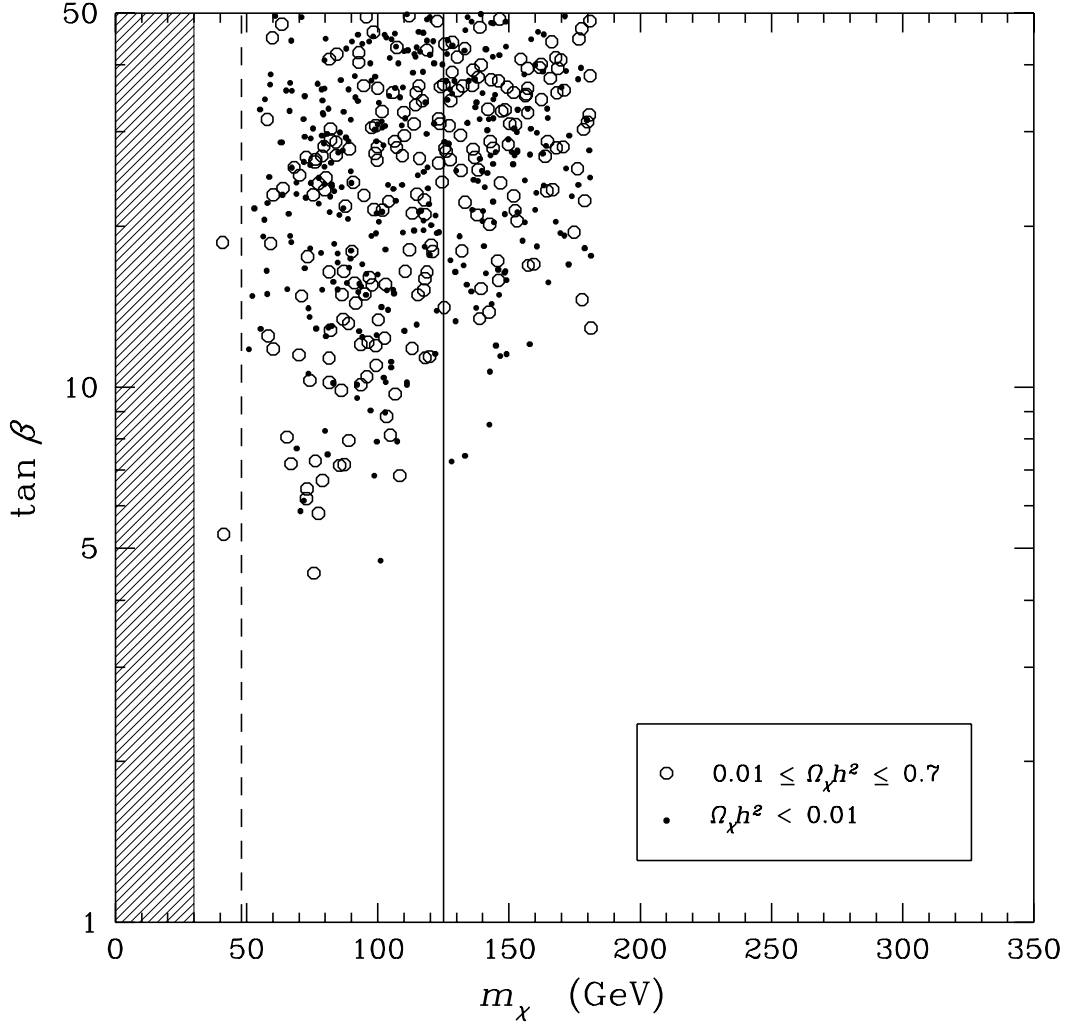


FIG. 7. Scatter plot for set  $S$  in the plane  $m_\chi - \tan \beta$ . The hatched region on the left is excluded by present LEP data. The dashed and the solid vertical lines denote the reach of LEP2 and TeV33, respectively.